CFD Modeling of Reactive Pollutants Dispersion in Simplified Urban Configurations with Different Chemical Mechanisms

Beatriz Sanchez[1], Jose-Luis Santiago[1], Alberto Martilli[1], Magdalena Palacios[1], and Frank Kirchner[2]

[1]Research Center for Energy, Environment and Technology (CIEMAT), Madrid, Spain
[2]GAIASENS Technologies. Sarl, Switzerland

Correspondence to: Beatriz Sanchez (beatriz.sanchez@ciemat.es)

Abstract. An accurate understanding of urban air quality requires considering a coupled behavior between dispersion of reactive pollutants and atmospheric dynamics. Currently, urban air pollution is mostly dominated by traffic emissions, being nitrogen oxides (NO_x) and Volatile Organic Compounds (VOCs) the primary emitted pollutants. However, modeling reactive pollutants with a large set of chemical reactions using a computational fluid dynamics (CFD) model requires a large amount of computational time. In this sense, the selection of the chemical reactions needed in different atmospheric conditions becomes essential to give the best compromise between CPU time and accuracy. The purpose of this work is to assess the differences in NO and NO_2 concentration considering three chemical approaches: a) passive tracers (non-reactive), b) the $NO_x - O_3$ photostationary state, and c) a reduced complex chemical mechanism based on 23 species and 25 reactions. The appraisal of the effects of chemical reactions focuses on studying the NO and NO_2 dispersion in comparison with the tracer behavior within the street. In turn, the effect of including VOC reactions is also analysed taking into account several VOC/NO_x ratios of traffic emission. Given that the NO and NO_2 dispersion can also be affected by the atmospheric conditions such as wind flow or the background concentration from season-dependent pollutants, in this work, the influence of wind speed and background O_3 concentration are studied. Results show that the presence of ozone in the street takes an important role in NO and NO_2 concentration. Therefore, greater differences linked to the chemical approach used are found with higher O_3 concentration and faster wind speed. This bears relation to the vertical flux as a function of ambient wind speed, since it increases the pollutants exchange between the street and the overlying air. This detailed study allows to ascertain under which atmospheric conditions the inclusion of chemical reactions are necessary for the study of NO and NO_2 dispersion. The conclusions can be applied to future studies in order to establish the chemical reactions needed in terms of an accurate modeling of NO and NO_2 dispersion and the CPU time required in a real urban area.

1 Introduction

Urban air pollution is nowadays a serious environmental problem. The non-uniformity in the buildings distribution in a city involves complex flow patterns and therein, heterogeneous pollutant dispersion within the streets. In addition, the high levels of detrimental pollutants in urban areas are mostly dominated by traffic emissions. The main related-traffic pollutants are NO_x ($NO + NO_2$), CO, hydrocarbons and particles. But given the proximity between sources and receptors in the street,

only the fastest chemical reactions have an impact on pollutants concentration. So some slow reactive compounds like CO or hydrocarbons can be considered as practically inert species at microscale. However, the NO_2 dissociation in presence of light and the NO titration by reduction of O_3 take place rather fast (Vardoulakis et al., 2003). And besides, Volatile Organic Compounds (VOCs) are also involved in this complex chain of reactions.

Currently, modeling urban air quality using a computational fluid dynamics (CFD) model is a big challenge. Besides pollutants dispersion, the simulation of chemical conversions of reactive pollutants in complex urban areas increases the computational time considerably. To better understand the problem, it is firstly necessary to thoroughly study the basic dynamical effects controlling non-reactive pollutants dispersion in simplified geometries. Many previous studies have investigated the main factors that affect the passive tracers distribution within the canopy such as the inflow conditions (Tominaga and Stathopoulos, 2010; Kim and Baik, 2004), the street-canyon aspect ratio (Chang and Meroney, 2003), thermal effects of a heating surface (Park et al., 2012) or the vegetation location in the street (Buccolieri et al., 2011).

However, the main pollutants in an urban area are largely reactive compounds and for that reason, the photostationary scheme was included in an attempt to examine the dispersion of pollutants in street canyons. Baker et al. (2004) and Baik et al. (2007) studied the dispersion of reactive pollutants in a street canyon considering the NO_x-O_3 photostationary steady state. Baik et al. (2007) also incorporated a heating surface at the bottom of the street and found that the magnitude of the chemical term for O_3 was comparable to the advection or turbulent diffusion terms, but that was not the case either for NO or for NO_2. Both researches showed that the O_3 concentration was faster depleted within the canopy because of the high NO emission at ground level. These studies underlined the importance of including the O_3 photochemical reaction in order to analyze the NO and NO_2 dispersion.

In addition, the VOCs related to traffic emission are also involved in urban air pollution. This becomes necessary to model a vast number of chemical interactions NO, NO_2, O_3 and VOCs. In more recent studies, complex chemical mechanisms have been implemented in CFD models in order to reproduce the NO and NO_2 dispersion in a street canyon. Kwak and Baik (2012) developed a CFD model coupled with the carbon bond mechanism IV (CBM-IV) and they evaluated the O_3 sensitivity with respect to different VOC and NO_x emission levels in a street canyon. They found that the O_3 removal from the NO reaction was more important than the NO_2 photolysis given by the continuous and high NO emission from vehicles, which causes that the O_3 behavior had a negative correlation with NO_x emission level. Likewise, the O_3 concentration was weakly correlated with the amount of VOC emission. Kwak et al. (2013) examined the dispersion and photochemical evolution of reactive pollutants in a street canyon with different canyon aspect ratios. It confirmed the relation O_3 with NO_x and VOC emission levels. And they found a slight influence of wind speed whereby increasing the wind speed enhances the exchange with overlying air which strengthens the downward O_3 transport. These recent studies highlight the importance of the O_3 oxidation process as well as the OH oxidation process in describing the photochemical reactions in the street. Park et al. (2015) analyzed different aspect ratios and several VOC/NO_x emission scenarios in three-dimensional street canyons. The main effects of NO_x and VOC emission levels in O_3 concentration are similar to the results obtained in two-dimensional studies. In contrast, small variations are locally found owing to different flow patterns generated by the geometry of the domain.

To further analyze the sensitivity with the chemical mechanism used in a CFD model, Kim et al. (2012) compared the hourly concentration of NO, NO_2 and O_3 with the photostationary steady state and a full chemical mechanism (110 species and 343 reactions) with identical conditions. The results revealed similar values of NO and NO_2 concentration, whereas the O_3 concentration with the simple mechanism was lower than that obtained with the full scheme. Bright et al. (2013) compared the O_3-NO_x chemical system with a full chemical mechanism (51 chemical species and 136 reactions) using a LES model. They studied in depth the effects of VOC chemical processes and found that by means of a more detailed chemistry, the values of NO, NO_2 and O_3 differ from the photostationary steady state, which reflects additional transformation of NO into NO_2 resulting from the intrinsic VOC degradation processes.

The coupled behavior between chemistry and dynamic processes is also a research goal. The relative importance of chemistry versus turbulent transport have been also investigated for homogeneous surface layers in the past (Galmarini et al., 1997; Molemaker and Vilà-Guerau de Arellano, 1998). The relative differences between turbulent and chemical time scales were evaluated using the Damkholer number. However, we estimate that this approach is not appropriate in the urban canopy layer (UCL). Basically because the transport is not only turbulent (as it is in the homogeneous surface layer), but also driven by the mean motions induced by the presence of the obstacles. Instead of adding a new time scale - linked to the mean transport - and trying to deal with the strong heterogeneity of the flow and associated time scales typical of the UCL, we found it more straightforward to perform simulations with and without chemical reactions, and to assess the relative importance of chemistry based on the difference between the simulations. In turn, regarding to the chemical scheme used, the best compromise between accuracy and CPU time required is also part of the main conclusions, since a complex chemical scheme implies more than twice the CPU time needed for the photostationary steady state.

Therefore, the aim of this work is to determine in which conditions result essential to incorporate more chemical reactions in order to model the dispersion of NO and NO_2 in the urban canopy. To achieve this goal, the NO and NO_2 dispersion is studied in two simplified geometries (2D and 3D geometries) under different chemical approaches: (a) non-reactive, (b) with photostationary steady state and (c) with a reduced complex chemical scheme (25 reactions and 23 species). In addition, knowing the impact of atmospheric conditions on reactive pollutants dispersion, the effects of the background O_3 concentration, the wind speed and the VOC/NO_x emission ratio are jointly assessed.

2 Chemical Schemes Used

The evaluation of NO and NO_2 dispersion regarded as reactive pollutants is here studied using two chemical schemes: the photostationary steady state and a reduced complex chemical scheme (CCM-CFD). The photostationary steady state is the most simple chemical mechanism implemented in the CFD and it is defined by a three-reaction system of NO, NO_2 and O_3.

$$NO_2 + h\nu \longrightarrow NO + O \quad \text{(R1)}$$

$$O + O_2 + M \longrightarrow O_3 + M \quad \text{(R2)}$$

$$O_3 + NO \longrightarrow NO_2 + O_2 \quad \text{(R3)}$$

Where M represents a molecule that absorbs excess energy and thereby stabilizes O_3 molecule formed (Seinfeld and Pandis, 1998). In the photochemical reaction, the photolysis rate constant is dependent on zenith angle (θ) and it is defined as $J_{NO_2} = A\,exp(B/cos(\theta))$, where A and B are chemical constants.

The complex chemical scheme used, which involves the VOC interactions, needs to be as reduced as possible due to the large load of computational time required to simulate a vast number of chemical reactions using CFD modelling and the number of simulations needed to carry out this detailed study. The aim was to reduce the Regional Atmospheric Chemistry Mechanism (RACM) -with 77 species and 237 reactions (Stockwell et al., 1997)- as far as possible without losing much accuracy during the first 30 minutes of simulation for urban conditions in a boxmodel. The CCM-CFD was created applying the software CHEMATA (CHEmical Mechanism Adaptation to Tropospheric Applications) (Junier et al., 2005; Kirchner, 2005). A wide set of different urban pollution conditions was investigated and special emphasis was given to cases where the results for the RACM mechanism differ considerable from the results of the photostationary steady state. Three main manners of mechanism reduction are applied:

- Modification of the lumping groups: Several chemical similar RACM lumping groups are united to a new lumping group. For example, the RACM alkanes ETH, HC3, HC5 and HC8 are summed up in the new species ALK. The RACM olefins ETE, OLT, OLI are lumped to the new species OLE and the RACM aromatic compounds TOL and XYL are integrated in the new species ARO.

- Modification of the organic peroxy radical parametrisation: instead of using the 20 RACM RO2 species, we applied the approach described by Kirchner (2005) with the RO2 species CH3O2 (called MO2) and RC(O)O2 (called ACO3) as well as the two operator species XO2 and XO2N which work in the following way. The real reactions:

$$R - H + HO \longrightarrow R^* + H_2O \quad \text{(R4)}$$

$$R^* + O_2 \longrightarrow RO_2 \quad \text{(R5)}$$

$$RO_2 + NO \longrightarrow a\,RONO_2 + b\,(RO + NO_2) \quad \text{(R6)}$$

$$RO \longrightarrow Products \quad \text{(R7)}$$

  are parameterised by;

$$R - H + HO \longrightarrow a\,XO_2N + b\,(XO_2 + products) \quad \text{(R8)}$$

$$XO_2 + NO \longrightarrow NO_2 \quad \text{(R9)}$$

$$XO_2N + NO \longrightarrow RONO_2 \quad \text{(R10)}$$

- Elimination of reactions and species which are not crucial for simulating under the given conditions (time scale of about 30 minutes, urban pollution conditions, daytime). Focusing on daytime simulations we can eliminate the species NO_3 and all its reactions. Also, low reactive species as CH_4 and H_2 can be eliminated under urban conditions.

The resulting CCM-CFD mechanism consists on 23 species and 25 chemical reactions (Table 1). Compared to the photostationary steady state, the CCM-CFD includes the peroxy radical production from VOCs, CO and SO_2 as well as NO_x loss processes by the formation of PAN, HNO_3 and organic nitrates. Whereas the peroxy radical production increases the NO_2/NO ratio as therefore the NO_2 concentrations, the NO_x loss processes decrease NO_x and therefore NO_2. As well, O_3 loss by the reaction with olefins is considered. Therefore, the effect on NO and NO_2 concentration after including the $O_3 - NO_x$ reactions can be quantified with the deviation from the non-reactive pollutant concentration. And besides, the influence of including reactions involving VOCs can be obtained by the differences on NO and NO_2 concentration between using the CCM-CFD and the photostationary steady state.

3 CFD Model Description

3.1 Model Description

The CFD model used is based on the Reynolds-averaged Navier-Stokes equations (RANS) with a k-ε turbulence model. This model allows to evaluate the effect of several parameters using a wide set of simulations within a reasonable CPU time. The turbulence can be solved more accurately by other models such as Large Eddy Simulation or Direct Numerical Simulation, however the CPU load increases considerably and it would limit the number of simulations. In this work, the CFD-RANS model is STARCCM+ (from CD-ADAPCO). It has been used in previous researches in order to study dynamical processes, thermal forcing and passive tracers dispersion in simplified and real urban geometries (Santiago and Martilli, 2010; Martilli et al., 2013; Santiago et al., 2014).

The NO_x-O_3 photostationary state and the complex chemical mechanism described in previous section are implemented in the CFD model, in a way that the chemical term is added to the transport equation for each pollutant. The chemical term is defined as formation and depletion of a compound in the chemical reactions and modeled as a production rate in the transport equation for each chemical specie ($[\Delta C]_{Chem}$). The traffic emission is added like a source term (S_{C_i}). Hence the transport equations are given by,

$$\frac{\partial C_i}{\partial t} + U_i \frac{\partial C_i}{\partial x_j} = D \frac{\partial^2 C_i}{\partial x_j \partial x_j} + \frac{\partial}{\partial x_j}\left(K_c \frac{\partial C_i}{\partial x_j}\right) + \left[\Delta C\right]_{Chem} + S_{C_i} \quad (1)$$

Where C_i is the concentration of the ith specie and D and K_c are molecular diffusivity and eddy diffusivity of pollutants, respectively.

3.2 Simulation Setup

The distribution and the residence time of pollutants in the streets are mainly affected by the flow defined as a result of buildings configuration. The pollutant dispersion is analyzed in two types of geometries with the purpose of understanding the behavior of reactive pollutants in the street and the dependence on geometry. Figure 1 shows the computational domains used: a single street-canyon (2D-geometry) and a staggered array of cubes (3D-geometry). The domain sizes of street-canyon and staggered array of cubes are 24x40x64 m and 64x64x64 m in x, y and z directions respectively. The aspect ratio defined as the ratio of

building height (H) to the street width (W) is $H/W = 1$ in both geometries. The top of the domains is fixed at 4H based on the results obtained in Coceal et al. (2006). The three-dimensional array of cubes is represented by staggered cubes with buildings width (L), resulting a packing density λ = 0.25. A grid independence test was carried out and the mesh resolution was selected to 1 m in all directions.

Symmetry boundary conditions are assumed in the spanwise direction (y-direction) and cyclic boundary conditions are imposed in the streamwise direction in order to simulate an infinite number of streets. The flow is driven in x-direction by a pressure gradient equal to $\rho u_\tau^2/4H$, where u_τ is a reference velocity. Two velocities are studied in this work, u_τ=0.45 m s^{-1} and u_τ=0.23 m s^{-1}. For u_τ=0.23 m s^{-1}, the corresponding wind speeds at 1.5H are 1.9 m s^{-1} and 1.5 m s^{-1} in the 2D and 3D geometries respectively, and the double for the u_τ=0.45 case. For flow and turbulence equations, symmetry conditions are established at the top of the domain that enforce parallel flow and zero normal derivatives for the dynamic variables (Santiago and Martilli, 2010).

The traffic emission sources are located at ground level in both domains (Fig.1). Knowing that the diurnal variation of traffic flow in an urban area registers two peaks of traffic around 08:00 LST and 20:00 LST and a valley around 13:00 LST, we focus on analyzing the NO and NO_2 dispersion in maximum emissions conditions at 08:00 LST. The traffic emissions are simulated considering a NO_x emission of 0.5 g km^{-1} per vehicle (Baker et al., 2004; Baik et al., 2007) and the volumetric ratio of NO and NO_2 emission is 10:1 (Buckingham, 1997). The NO and NO_2 emissions are fixed with rates of 112 µg $m^{-1}s^{-1}$ and 17 µg $m^{-1}s^{-1}$ respectively, which is equivalent to 930 vehicles per hour representative of medium traffic (Baker et al., 2004). In addition, the VOC traffic emissions are included on using the CCM-CFD. The emitted VOC/NO_x ratio by vehicles is dependent on several factors such as kind of vehicle or traffic flow speed. For that, two VOC/NO_x emission ratio are simulated: 1/5 and 1/2, which are within the typical values of traffic emission ratio in last years of Madrid city (Ayuntamiento-Madrid, 2014). Some VOC are lumped in terms of specific functional groups in the CCM-CFD. The emitted VOC species are OLE, ARO, ALK, ALD and HCHO, and their volumetric proportions are 28.6 %, 23.1 %, 38.6 %, 4.0 % and 5.6 %.

For transport equations of pollutants, constant concentrations are established as boundary conditions at the top of domain. Due to cyclic and symmetry conditions along x-direction and y-direction respectively, these concentrations play an important role considering chemical reactions and the background concentrations of pollutants are imposed. The values of NO, NO_2, CO and SO_2 concentrations are fixed at 16, 35, 200 and 2 ppb for all scenario. However, the VOC concentrations are established with the same VOC/NO_x emission ratio considered in that simulation. On the other hand, the estimation of the O_3 concentration (hereafter, referred as $[O_3]$) at the top is computed by the photochemical equilibrium equation,

$$[O_3] = \frac{J_{NO_2}[NO_2]}{k[NO]} \tag{2}$$

where k is the rate reaction constant and it is set assuming isothermal condition (T=298 K). With the purpose of evaluating the influence of the available O_3 on NO and NO_2 concentration (hereafter referred to as [NO] and $[NO_2]$) within the street, two characteristic cases of opposite seasons are studied. The photolysis rate J_{NO_2} is calculated as a function of the zenith angle, hence a representative zenith angle of winter (θ=78°) and another one of summer (θ=46°) are considered to compute the $[O_3]$

established at top of the domain. The resulting background $[O_3]$ are 10.6 and 39.8 ppb for the representative cases of winter and summer respectively.

Table 2 summarizes all simulated cases in each computational domain: 2D and 3D geometry. The pollutants dispersion is analyzed considering the following chemical scenarios: (a) non-reactive pollutants, (b) NO_x-O_3 photostationary state, (c) CCM-CFD with VOC/NO_x=1/5 and (d) CCM-CFD with VOC/NO_x=1/2. And the four chemical scenarios are simulated in every atmospheric conditions combining two reference velocities (u_τ=0.45 m s^{-1} and u_τ=0.23 m s^{-1}) and two ozone background concentrations ($[O_3]$=10.6 ppb and $[O_3]$=39.8 ppb).

3.3 CFD Model Evaluation

Due to a lack of experimental data that can be used to evaluate the chemical mechanisms, the results from the CFD model are evaluated in two steps. Firstly, the dispersion in the canyon using the non-reactive case is compared with experimental data (Meroney et al., 1996). Secondly, the implementation in the CFD model of the chemical terms as a part of the complex chemical scheme (CCM-CFD) is evaluated with the results from a chemical box model well-established (Junier et al., 2005; Kirchner, 2005).

The non-reactive pollutant dispersion is evaluated with wind tunnel experimental data (Meroney et al., 1996). The experimental system consists on a single 2D street canyon with $H/W = 1$. The wind blows perpendicular to the canyon in x-direction and the emission source is located at the bottom of the domain. This scenario is similar to our 2D-CFD simulations with the exception of the cyclic boundary conditions imposed in streamwise direction. In the comparison with experimental data, the inlet concentration is dismissed from the concentration inside the canyon. We focus on comparing pollutant concentration from simulation results with the measurements of urban roughness experimental case at different points close to walls within the canyon (Fig. 2). The concentration at each measurement point is normalized with respect to the concentration at the point 7 within the street (C/C_7). The same normalization was used in Santiago and Martín (2008) to evaluate the CFD model results with same experiment. Comparison between experimental and computed normalized concentration is depicted in Fig. 3.

Overall, a good agreement is obtained in spite of the slight difference at point 4 and 13 where the concentration is lower than experimental data. Besides the linear regression concludes a good correlation (R=0.92) between experimental measurements and simulated results. For further information, the statistical parameters of Normalized Mean Square Error (*NMSE*), Fractional BIAS (*FB*), correlation (*R*) and the fraction of predictions within a factor of 2 of observations (*FAC2*) are computed following the equations,

$$NMSE = \frac{\sum_{i=1}^{n}(O_i - P_i)^2}{\sum_{i=1}^{n}(O_i P_i)} \tag{3}$$

$$FB = \frac{\overline{O} - \overline{P}}{0.5(\overline{O} + \overline{P})} \tag{4}$$

$$R = \frac{\sum_{i=1}^{n}[(O_i - \overline{O})(P_i - \overline{P})]}{\left[\sum_{i=1}^{n}(O_i - \overline{O})^2\right]^{1/2}\left[\sum_{i=1}^{n}(P_i - \overline{P})^2\right]^{1/2}} \tag{5}$$

$$FAC2 = \text{fraction of data that satisfy } 0.5 \leq P_i/O_i \geq 2 \tag{6}$$

Where *n* is the number of points, the O_i are the measurements at each point, and $\overline{O}$ is the measurement mean. And P_i and $\overline{P}$ are the computed values at each point and its corresponding mean. The values of *FAC2*=1, *NMSE*=0.030 and *FB*= 0.068 reveal a good fit between computed and experimental data with a slight underestimation. Therefore, the pollutant dispersion is accurately simulated in base to the model acceptance criteria established for *NMSE*<1.5 and -0.3<*FB*<0.3 in Chang and Hanna (2005) and as a threshold of the correlation coefficient *R*>0.8 in Goricsán et al. (2011) (Table 3).

Secondly, the accuracy of solving a vast number of chemical reactions using the CFD model is evaluated with the chemical box model used to develop the CCM-CFD (Section 2). For this comparison, the CFD model was run as a box and the chemical evolution for the reactive species of the CCM-CFD is simulated during 30 min. Similar initial conditions and the related-traffic pollutant emissions of an urban area are considered in this test. In both cases, the reaction rate and the photolysis rate constants are fixed using, *T*=293 K and θ=40°. In a detailed assessment, the statistical parameters *NMSE*, *FB*, *R* and the maximum relative concentration error from the CFD results with respect to the box model results are calculated for all pollutants. The *NMSE* and *FB* indicate that the CFD results of concentration are quite similar to the box model results, with values of the order 10^{-6} and 10^{-3} respectively, and the correlation is approximately 1 for all pollutants. As well, for instance, the maximum relative error of concentration for NO, NO_2 and O_3 is 0.28 %, 0.18 % and 0.085 % respectively. These differences are mainly caused by numerical errors. Therefore, the implementation of the chemical terms in the transport equations in the CFD model is appropriately solved.

Lastly, the appropriate time step in order to solve the dynamic transport and the chemical reactions is evaluated using the CCM-CFD with VOC/NO_x=1/2 in 2D-geometry. The concentration of reactive pollutants is analyzed for different time steps (0.1 s, 1 s and 2 s). During the first period of the simulation, the turbulent dynamic is simulated a time step of 1s, without including chemical interactions. After that, the chemical reactions are implemented in the CFD simulation carrying out every time step case (t_s=0.1 s, t_s=1 s and t_s=2 s). Finally, when the steady state is reached, the horizontal spatial average concentrations of NO, NO_2 and O_3 are compared in the whole domain. The deviation of concentration from the case with t_s=1 s is quantified using the quadratic relative differences given by,

$$QD(\%) = \frac{\sqrt{\frac{1}{n}\sum_{k}^{n}(C'_k - C_k)^2}}{\frac{1}{n}\sum_{k}^{n} C_k} \cdot 100 \tag{7}$$

where C'_k and C_k is the horizontal average concentration at several vertical levels with t_s=0.1 s or 2 s and t_s=1 s, respectively. The results of the *QD* for NO, NO_2 and O_3 from the simulations with the time step 0.1 s and 2 s are enclosed in Table 4. By comparing these results, we establish the time step at 1 s in order to simulate the dispersion of reactive pollutants.

4 Results and discussion

The CFD model is used to simulate turbulent flow and dispersion of reactive species in two different geometries: a 2D street canyon and a 3D staggered array of cubes. The interaction between the atmosphere and buildings configuration induces complex flow patterns within the urban canopy and this induces a heterogeneous pollutant distribution in the streets. Herein the canopy height is regarded as the height of buildings (H). The ventilation of the street in a 2D-geometry is more reduced than in a 3D-geometry and accordingly, pollutants reside longer in the street (Vardoulakis et al., 2003). Thus, the residence time of pollutants in the street is determined by building configurations and wind flow. The time that these pollutants remain within the street affects to the chemical interactions, and as a consequence, to the amount of concentration at pedestrian level. For that reason, the effects of including chemical reactions in the CFD simulations are evaluated in 2D and 3D domains. To facilitate the analysis, the concentration of the study pollutants are normalized using the emission area (A_{Em}), the reference velocity (u_τ) and the source emission rate (Q) given by,

$$C_N = \frac{C\, u_\tau\, A_{Em}}{Q} \tag{8}$$

This work is focused on analyzing NO and NO_2 dispersion within the street and their normalized concentration are referred as $[NO]_N$ and $[NO_2]_N$. In addition to quantify the effect of considering chemical reactions, the deviation in concentration (δC) from the non-reactive compound behavior is computed as,

$$\delta C(\%) = \frac{C_N - C_N(T)}{C_N(T)} \cdot 100 \tag{9}$$

where C_N and $C_N(T)$ are the normalized concentration of the pollutants regarded as reactive and non-reactive, respectively.

4.1 Ozone Influence on Reactive Pollutants.

The O_3 concentration is generally dependent on the photochemical regime but in the street, it is also affected by chemical interactions with the NO_x and VOC levels owing to the VOC-NO_x traffic emission ratio. Kwak and Baik (2012) analyzed the effect of several VOC-NO_x emission ratios with a background $[O_3]$ fixed. In addition, with NO_x-VOC fixed emission rates, the diurnal variation of NO_x and the exchange of O_3 at roof level was studied in Kwak and Baik (2014). To further examine the influence of the available O_3 on [NO] and $[NO_2]$ in the street with several levels of VOC emission, two background $[O_3]$ are considered: Case 2 and Case 4 (Table 2).

Figure 4 shows δNO and δNO_2 in the 2D geometry. In the case with lower $[O_3]$ of background, either considering the photostationary steady state (hereafter referred to as PSS) or the CCM-CFD with VOC/NO_x emission ratio 1/5 or 1/2 (hereafter referred to as CCM1/5 and CCM1/2), δNO and δNO_2 below the canopy top are around 3 % and 30 % respectively. This indicates that the reactions involving VOC have little impact on the NO and NO_2 levels, whereas the $NO_x - O_3$ reactions have a slightly major effect on $[NO_2]$. On the other hand, in the higher O_3 case, δNO and δNO_2 increase in average to nearly 12.5 % and more than 100 % inside the street respectively, and besides the difference of including VOC reactions is remarkable. As a result, in the higher O_3 case and high VOC emission, the $[NO_2]$ and [NO] in the street is respectively underestimated and overestimated with the PSS in comparison with the results including the VOC reactions.

The $[NO]_N$ and $[NO_2]_N$ from PSS, CCM1/5 and CCM1/2 are compared in normalized concentration with their corresponding non-reactive pollutant below the canopy top in the 2D and 3D geometries. Figure 5 illustrates the vertical profiles of the horizontal spatial average of $[NO]_N$ and $[NO_2]_N$ for the two O_3 cases. In the lower O_3 case, the difference between chemical scenarios is negligible in both computational configurations. Overall, the variation of $[NO]_N$ and $[NO_2]_N$ among PSS, CCM1/5 and CCM1/2 are bounded on 0.05 % and 2.3 %, which represents a maximum deviation of 0.3 and 1.3 ppb in absolute concentration within the street respectively. In contrast, in the higher O_3 case, the importance of the photochemical reactions increases. In 2D-geometry, with the PSS, CCM1/5 and CCM1/2, the $[NO]_N$ is respectively about 10.1 %, 10.5 % and 12.3 % less than the normalized tracer concentration within the canopy in the street canyon geometry. Likewise in the 3D-geometry, the $[NO]_N$ for all mechanisms are shifted around 10-12 % from non-reactive pollutant. Focusing on $[NO_2]_N$ including VOC reactions against the $NO_x - O_3$ system, NO_2 is more affected by the increase of the background O_3 and the photochemical reactions owing to the zenith angle of summer. The $[NO_2]_N$ rises more than 15 % with CCM1/2 which represents values of up to 10 ppb in the 2D configuration and 7 ppb in the staggered array of cubes. Therefore, in both geometries, the $[O_3]$ of background and the solar position (θ) regarded in photolysis rates highlight the effect of including more chemical reactions on the study of NO and NO_2 dispersion in the street.

In addition, the difference among chemical mechanisms is also influenced by VOC levels. In the lower O_3 case, the effect of VOC emissions have a minimum impact on $[NO]_N$ and $[NO_2]_N$. That is due to the selected zenith angle is representative of winter conditions, therefore the photolysis constants are smaller than that given in a representative summer case. This implies that the background O3 concentration computed by the photochemical equilibrium equation is low. In turn, the VOC oxidation cycle is also limited by the photolysis of some VOCs. Besides, given that the NOx emissions dominate over the VOC emissions, the high levels of NOx concentration tend to inhibit O3 formation and limit the O3 production through VOC reactions. Therefore, the difference in NO and NO2 concentration after including VOC reactions against the photostationary steady state is negligible in this low O3 case. So the weak dependence on VOC concentration is a combination of the low O3 and small photolysis rates. And therefore, the PSS or a more complex chemical mechanism can be used to reproduce the NO and NO_2 dispersion in the street since the results are quite similar. However, in the representative summer case with high VOC levels, the reactions involving VOC are more important and larger differences in [NO] and $[NO_2]$ with respect to NO_x-O_3 system are found. For instance in 2D-geometry, $[NO]_N/[NO(T)]_N$ is 0.87, 0.89 and 0.90 whereas $[NO_2]_N/[NO_2(T)]_N$ varies from 2.18, 2.03 and 2.01 for CCM1/2, CCM1/5 and PSS respectively. Concluding that taking into account the VOC reactions, the NO production is reduced and NO_2 retrieval is increased in comparison to the results from the PSS owing to the degradation of VOC. This effect is remarkable in the higher $[O_3]$ case and high VOC traffic emissions.

4.2 Wind speed influence on reactive pollutants

The concentration of a non-reactive pollutant is inversely proportional to wind speed (Parra et al., 2010), but the non-linearity of chemical reactions induces changes in this behavior. The effect due to wind speed on NO and NO_2 dispersion is obtained considering two wind speeds changing the reference velocity (u_τ): Case 1 and Case 2 (Table 2). As discussed in the previous

section, the higher O_3 case is used in this section given that chemical reactions have more effect on NO and NO_2 concentrations below the canopy top.

Figure 6 shows the δNO and δNO_2 for different values of wind speed in the 2D-geometry. In the faster wind speed case, the differences on normalized concentration are larger in comparison to the tracer behavior. Overall, for all chemical scenarios, $[NO]_N$ is reduced from the tracer around 18 % and 10% within the canopy with u_τ=0.45 m s^{-1} and u_τ=0.23 m s^{-1} respectively. However, the $[NO_2]_N$ increases a factor 2.7 and 2 from the normalized tracer concentration for u_τ=0.45 m s^{-1} and u_τ=0.23 m s^{-1}, respectively. Therefore, greater influence of chemical reactions on NO and NO_2 dispersion is obtained with the faster wind speed since it increases the O_3 inflow to the street acting as a trigger between pollutant interactions. Note that for a tracer, the normalized concentration is proportional to concentration and inversely proportional to wind speed. However, the behavior of the normalized concentration of a reactive pollutant is not lineal with the wind speed.

To analyze the [NO] and $[NO_2]$ within the canopy, the vertical profiles of horizontal spatial average of the normalized concentration in the 2D and 3D geometries are depicted in Fig. 7. Different vertical distributions of the normalized concentration are obtained for each geometry. However, the same deviation of the normalized concentrations including chemical reactions from its corresponding tracer is obtained in the 2D and 3D geometries with different wind speed. In the faster wind speed case, the normalized concentration tends to be further from the non-reactive normalized concentration, however the variation among chemical scenarios is small. The $[NO]_N$ and $[NO_2]_N$ with CCM1/2 just differ from PSS around 1% and 7% respectively. In contrast, with lower wind speed, the $[NO_2]_N$ with CCM1/2 and CCM1/5 increases 17% and 2% respectively from the PSS. In this case, the accumulation of NO_x emissions within the street is greater, which contributes to quickly consume the $[O_3]$, reducing the NO_2 production and the NO removal. Likewise, the VOC levels given by the increase of emissions in the street intensify the NO_2 production and NO depletion, developing the opposite effect. This means that the concentration from reactive pollutants is higher with faster wind speeds since it produces a greater exchange of pollutants between the street and overlying air. Whereas when the wind speed is reduced, the difference from tracer behavior is reduced but, the importance of reactions involving VOC increases in comparison with just regarding the $NO_x - O_3$ system.

4.3 Vertical transport

The vertical transport of NO, NO_2 and O_3 is analyzed in both geometries in order to determine the atmospheric conditions as from which the use of VOC reactions is needed to accurately reproduce the NO and NO_2 dispersion within the street. With this analysis, it is possible to understand how either wind speed or the background of $[O_3]$ affect on pollutants concentration. Figure 8 shows the average of the deviation of $[NO]_N$ and $[NO_2]_N$ below the canopy top in comparison to their corresponding tracer in each geometry (Eq. 9). For all cases simulated, the similar deviation of NO and NO_2 from its tracer is obtained in both geometries.

In the lower O_3 case, the differences on δNO and δNO_2 among chemical mechanisms in 2D-geometry are negligible even with different wind speeds. For all chemical scenarios, δNO is around 5 % and 3 % for u_τ=0.45 m s^{-1} and u_τ=0.23 m s^{-1}, respectively. However, in the higher O_3 conditions, the differences of the simple scheme and by including VOC reactions are greater and the dependency with the wind speed is significant. As it has seen before, despite of the deviation in comparison

with tracer is larger with the u_τ=0.45 m s^{-1}, the higher differences between chemical scenarios are obtained with u_τ=0.23 m s^{-1}. The maximum differences on $[NO]_N$ and $[NO_2]_N$ are obtained with more VOC emissions, and their variation switch from 10 % to 20 % when the inflow velocity changes of u_τ=0.45 m s^{-1} to the half. Therefore, the chemical reactions are strongly determined by the available O_3 of background and subsequently, they have an slight dependency with the wind speed.

With the objective to deepen on the exchange of ozone inflow into the street, the vertical fluxes are analyzed. Given that, there are only small differences between both computational domains with the same aspect ratio H/W=1. The pollutant removal from the street and pollutant entrainment into the street are analyzed by means of vertical fluxes of NO, NO_2 and O_3 in the 3D-geometry. The total vertical flux ($F_{T,i}$) is defined as a sum of vertical mean flux ($F_{m,i}$) and turbulent flux ($F_{t,i}$). The horizontal spatial average (<>) of $F_{T,i}$ of ith species is computed at several vertical levels every 1 m using the following equations.

$$F_{T,i} = <\overline{wC}> = F_{m,i} + F_{t,i} \tag{10}$$

$$F_{m,i} = <\overline{w}\,\overline{C_i}> \tag{11}$$

$$F_{t,i} = <\overline{w'C_i'}> = -K_c \frac{\partial C_i}{\partial z} \tag{12}$$

Here w and w' are the vertical velocity and its fluctuation respect to the mean, $\overline{w}$. And C_i and C_i' are the corresponding variables to the concentration of ith species. To examine the atmospheric parameters effect on NO and NO_2 regarded as reactive pollutants through vertical fluxes, the NO and NO_2 fluxes are normalized following the method developed for a passive tracer in Martilli et al. (2013). For a passive tracer, taking into account an homogeneous emission at surface, the steady state and neglecting vertical variations of air density with height, the following holds, within the canopy (Eq. 13) and above (Eq. 14).

$$<\overline{w'C'}> + <\overline{w}\,\overline{C}> = S \tag{13}$$

$$<\overline{w'C'}> + <\overline{w}\,\overline{C}> = S\,\frac{A_{street}}{A_{street} + A_{roof}} \tag{14}$$

Where S is the constant emission flux at the surface and A_{street} and A_{roof} are the areas of the streets and roofs of buildings respectively. Hereafter the spatial horizontal average of total fluxes of NO and NO_2 are normalized with S (within the canopy) and S $A_{street}/(A_{street} + A_{roof})$ above, referred as $<\overline{w\,NO}>_N$ and $<\overline{w\,NO_2}>_N$.

Figure 9 illustrates the vertical profiles of the deviation of $<\overline{w\,NO}>_N$, $<\overline{w\,NO_2}>_N$ from the normalized total flux of tracer and the vertical profile of $<\overline{w\,O_3}>$ spatially averaged for the CCM1/2 and PSS scenarios in the 3D-geometry. The CCM1/5 results are not shown since their results are quite similar to PSS results. The $<\overline{w\,NO}>_N$ and $<\overline{w\,NO_2}>_N$ taking into account chemical reactions are compared with the normalized flux of tracer. The vertical transport of a tracer above the canopy top is only turbulent, given that the mean vertical velocity is zero, but within the canopy in the middle part, it is mainly dominated by mean flux. This behavior is obtained for NO and NO_2 regarded as reactive pollutants as well. Unlike the tracer fluxes, the turbulent fluxes of NO and NO_2 are affected by chemical interactions, mainly with O_3. In Fig. 9, we can observe that the effect of the chemical reactions involving VOC (with the VOC/NO_x=1/2) on vertical transports of NO and NO_2 are significant in the higher $[O_3]$ and faster wind speed case. In this case, the $<\overline{w\,NO}>_N$ and $<\overline{w\,NO_2}>_N$ are slightly smaller and larger

respectively, corresponding to a greater vertical transport of O_3 in all heights and more photochemical activity. In contrast, in the other cases, the influence of introducing chemical reactions on $< \overline{w\,NO} >_N$ and $< \overline{w\,NO_2} >_N$ just can be observed above the canopy top whereas inside the street is quite similar to the tracer flux. That is due to fact that the $[O_3]$ is practically depleted by reaction with NO before entering into the street. Besides the strong NO emission and lower wind speed avoid the escape of NO from the street and block the O_3 formation by means of degradation reactions of VOC. That means that in the higher O_3 case with the faster wind speed, the downward motion contributes to introduce $[O_3]$ into the street and the upward motion remove the [NO] of the street. And moreover, the VOC emissions benefit the conversion of NO to NO_2. Therefore, the impact of the reactions involving VOC with the emission ratio VOC/NO_x=1/2 on [NO] and $[NO_2]$ is significant in the street .

For a better understanding of the relative importance of including more chemical reactions and so to characterize the NO and NO_2 dispersion under several conditions, the effect on $[NO]_N$ and $[NO_2]_N$ within the canopy is analyzed considering jointly all variables here studied. In this way, the variability of vertical transport of O_3 and in turn the effect of VOC emission, linked to the change of wind speed are examined. Figure 10.a shows the averaged concentration within the canopy of $[NO_2]_N$ over $[NO]_N$ in relation to the total flux of O_3 at roof level ($< \overline{w\,O_3} >_N$) for the PSS and CCM1/5 and CCM1/2 in the ozone and wind speed cases. Note that $[NO_2]_N/[NO]_N$ is 1 for the non-reactive species. Thus, the deviation from 1 indicates the effect of chemical reactions. Figure 10.b illustrates the variation of considering VOC reactions aside from the NO_x-O_3 reactions by means of $[NO_2]_N$ with respect to the increase of VOC average concentration below the canopy top.

In Fig. 10.a we can observe that the effect of chemical reactions is greater in the higher O_3. With faster wind speed, the inflow of O_3 to the street increases owing to the downward motion and for that, the value of $[NO_2]_N/[NO]_N$ is large. On the other hand, when the $[O_3]$ levels are not enough to react with large NO_x emissions and the photochemical reactions are slower, the difference on $[NO]_N$ and $[NO_2]_N$ with respect to the normalized concentration tracer is smaller ($[NO_2]_N/[NO]_N < 1.75$). Focusing on the lower O_3 case, the variation among chemical scenarios is negligible. However, higher differences are found on $[NO_2]_N/[NO]_N$ by increasing the inflow of $[O_3]$ into the street. The deviation on $[NO_2]_N$ after including VOC reactions against the photostationary steady state is analyzed in Fig. 10.b. The slight variations among chemical scenarios is just caused by VOC levels. Although the results conclude that small differences exist in winter conditions, they are insignificant since the maximum deviation is 1 ppb corresponding to the slow velocity for CCM1/2. In contrast, in summer case, with high $[O_3]$, the variations between chemical scenarios are greater and increase with the VOC emission in the street. That is due to the slower wind speed which induces less vertical exchange and avoids the exit of VOC concentration from the street. In fact the higher VOC emissions under these conditions benefit the VOC reactions, which induce the conversion of NO to NO_2, rising the difference with respect to the NO_x-O_3 reactions.

In summary, the impact of the chemical reactions below the canopy top is affected by the O_3 entrainment within the canopy. And this is directly proportional to the value of O_3 above the canopy top and the wind speed. On the other hand, the VOC reactions are more important in the canopy under high O_3 and high VOC levels. The second depends on the emission ratio and the upward VOC flux at the top of the canopy. For that, stronger winds will increase the flux, and so reduce the importance of the VOC reactions in the canopy.

5 Conclusions

The purpose of this work is to optimize the modeling of NO and NO_2 dispersion with respect to chemical reactions over a real urban area. Accordingly, an analysis of the relative importance of chemical reactions respect to mean and turbulent transport has been carried out by means of a CFD model. This is based on three different model set-ups: a simulation where chemical reactions are not considered (passive tracer), one where only the $NO_x - O_3$ cycle is simulated (Photostationary steady state), and the last one where the reactions involving VOC are also implemented (a Complex Chemical Mechanism reduced for the CFD model). With normalized concentration the source emission dependency is dismissed, and the deviation with respect to tracer is only due to the chemical reactions of pollutants with each other. As well, this helps to extract the conclusion in the 2D and 3D configurations used without dependence on geometry.

As it can be seen in this study, the general conclusions linked to the use of chemical reactions are obtained from both geometries. The solar position and the available O_3 within the canopy determine the impact on NO and NO_2 concentration in the street on including chemical reactions. Additionally, the influence of wind speed is evaluated in order to establish a relation of [NO] and $[NO_2]$ with $[O_3]$ below the canopy. The wind speed defines the vertical transport in the domain and consequently, the inflow of O_3 into the street. Based on this, the higher differences on $[NO]_N$ and $[NO_2]_N$ from the tracer are obtained with faster wind speed in the higher $[O_3]$ of background case. That is due to a major vertical exchange of concentration that intensifies the NO_x removal and the O_3 entrainment in the street. However in the winter representative case when the amount of O_3 is generally lower, the variation of wind speed has hardly influence on $[NO]_N$ and $[NO_2]_N$.

Given that the VOC are also emitted in traffic exhausts, two real emission ratios of VOC/NO_x are considered (VOC/NO_x=1/2 and VOC/NO_x=1/5). The vertical fluxes of concentration and the average concentration below the canopy under several atmospheric conditions show the deviation on $[NO]_N$ and $[NO_2]_N$ by including VOC reactions against to the $NO_x - O_3$ system. With high available ozone in the street, the difference between chemical schemes is intensified by increasing the amount of VOC emission. The lower wind speed conditions encourages the increment of VOC within the canopy and this bears relation to the NO reduction and NO_2 production, the canopy and the chemical interactions increase the NO conversion into NO_2. Likewise, the formation of O_3 related to the photolysis of NO_2 along with the O_3 concentration of background increase the difference on the $[NO_2]_N$ considering the VOC reactions with respect to the simple chemical mechanism.

Nowadays, the big concern about air quality in big cities is carrying out many studies about dispersion of the primary pollutants related to traffic emissions. It focuses on NO_2 since it is the most detrimental for citizens health. To simulate its dispersion in a real urban area is a big challenge from the perspective of modeling at microscale with a CFD model. To obtain the best compromise between accuracy and the CPU time required in order to simulate the NO_2 dispersion within the streets, this work seeks the chemical reactions needed as a function of several atmospheric conditions. In winter conditions when the O_3 concentration within the canopy is usually below 5 ppb and the solar radiation is low, the implementation of $NO_x - O_3$ reactions can be suitable with slight errors. For instance, the $[NO]_N$ and $[NO_2]_N$ for CCM1/2 and CCM1/5 differ from the PSS less than 2 $\%$. Even with a low wind speed, the behavior of $[NO]_N$ and $[NO_2]_N$ in average is quite close to that tracer. In contrast when the amount of the available O_3 within the street increases to more than 10 ppb within the canopy, the differences

linked to the chemical reactions considered rises. The non linearity of chemistry induces that [NO] and $[NO_2]$ are not inversely proportional with respect to wind speed, unlike the non-reactive pollutant. Moreover the VOC levels within the street is also an important factor to take into account. With conditions of high background O_3 concentration, and with an emission ratio of $VOC/NO_x = 1/2$, the $[NO]_N$ and $[NO_2]_N$ increase the error with respect to PSS more than 16 $\%$, hence the VOC chemical reactions seem to be necessary in order to reproduce the NO and NO_2 dispersion in the streets. These assumptions can be useful and provide information to study the pollutants dispersion in real urban areas using a CFD model.

Author contributions. B. Sanchez performed the CFD simulations. B.Sanchez, JL. Santiago and A. Martilli discussed the results from the CFD simulations and the conclusions. M. Palacios reviewed the chemical comments. F. Kirchner developed the complex chemical mechanism implemented in the CFD model. B. Sanchez prepared the manuscript with contributions from all co-authors.

Acknowledgements. This study has been supported by European Project LIFE MINOx-STREET (LIFE12 ENV/ES/000280) funded by EU. Authors thank Extremadura Research Centre for Advanced Technologies (CETA-CIEMAT) by helping in using its computing facilities for the simulations. CETA-CIEMAT belongs to CIEMAT and the Government of Spain and is funded by the European Regional Development Fund (ERDF).

References

Ayuntamiento-Madrid: Inventario de emisiones de contaminantes a la atmósfera en el municipio de Madrid 1999-2012 (in Spanish). Area de Gobierno de Medio Ambiente y Movilidad del Ayuntamiento de Madrid, Spain. (website: http://www.madrid.es/UnidadesDescentralizadas/Sostenibilidad/ EspeInf/EnergiayCC/04CambioClimatico/4aInventario/Ficheros /InventarioEAM2012.pdf), 2014.

Baik, J.-J., Kang, Y.-S., and Kim, J.-J.: Modeling reactive pollutant dispersion in an urban street canyon, Atmospheric Environment, 41, 934–949, 2007.

Baker, J., Walker, H. L., and Cai, X.: A study of the dispersion and transport of reactive pollutants in and above street canyons—a large eddy simulation, Atmospheric Environment, 38, 6883–6892, 2004.

Bright, V. B., Bloss, W. J., and Cai, X.: Urban street canyons: Coupling dynamics, chemistry and within-canyon chemical processing of emissions, Atmospheric Environment, 68, 127–142, 2013.

Buccolieri, R., Salim, S. M., Leo, L. S., Di Sabatino, S., Chan, A., Ielpo, P., de Gennaro, G., and Gromke, C.: Analysis of local scale tree–atmosphere interaction on pollutant concentration in idealized street canyons and application to a real urban junction, Atmospheric Environment, 45, 1702–1713, 2011.

Buckingham, C.: London atmospheric emissions inventory, London Research Centre, 1997.

Chang, C.-H. and Meroney, R. N.: Concentration and flow distributions in urban street canyons: wind tunnel and computational data, Journal of Wind Engineering and Industrial Aerodynamics, 91, 1141–1154, 2003.

Chang, J. C. and Hanna, S. R.: Technical descriptions and user's guide for the BOOT statistical model evaluation software package, Version 2.0, Available on harmo. org= Kit= Download= Kit_key. pdf, 2005.

Coceal, O., Thomas, T., Castro, I., and Belcher, S.: Mean flow and turbulence statistics over groups of urban-like cubical obstacles, Boundary-Layer Meteorology, 121, 491–519, 2006.

Galmarini, S., Vilà-Guerau De Arellano, J., and Duynkerke, P.: Scaling the turbulent transport of chemical compounds in the surface layer under neutral and stratified conditions, Quarterly Journal of the Royal Meteorological Society, 123, 223–242, 1997.

Goricsán, I., Balczó, M., Balogh, M., Czáder, K., Rákai, A., and Tonkó, C.: Simulation of flow in an idealised city using various CFD codes, International Journal of Environment and Pollution, 44, 359–367, 2011.

Junier, M., Kirchner, F., Clappier, A., and van den Bergh, H.: The chemical mechanism generation programme CHEMATA—Part 2: Comparison of four chemical mechanisms for mesoscale calculation of atmospheric pollution, Atmospheric Environment, 39, 1161–1171, 2005.

Kim, J.-J. and Baik, J.-J.: A numerical study of the effects of ambient wind direction on flow and dispersion in urban street canyons using the RNG k–ε turbulence model, Atmospheric Environment, 38, 3039–3048, 2004.

Kim, M. J., Park, R. J., and Kim, J.-J.: Urban air quality modeling with full $O_3 - NO_x - VOC$ chemistry: Implications for O_3 and PM air quality in a street canyon, Atmospheric Environment, 47, 330–340, 2012.

Kirchner, F.: The chemical mechanism generation programme CHEMATA—Part 1: The programme and first applications, Atmospheric Environment, 39, 1143–1159, 2005.

Kwak, K.-H. and Baik, J.-J.: A CFD modeling study of the impacts of NO x and VOC emissions on reactive pollutant dispersion in and above a street canyon, Atmospheric Environment, 46, 71–80, 2012.

Kwak, K.-H. and Baik, J.-J.: Diurnal variation of NO x and ozone exchange between a street canyon and the overlying air, Atmospheric Environment, 86, 120–128, 2014.

Kwak, K.-H., Baik, J.-J., and Lee, K.-Y.: Dispersion and photochemical evolution of reactive pollutants in street canyons, Atmospheric Environment, 70, 98–107, 2013.

Martilli, A., Santiago, J. L., and Salamanca, F.: On the representation of urban heterogeneities in mesoscale models, Environmental Fluid Mechanics, 15, 305–328, 2013.

Meroney, R. N., Pavageau, M., Rafailidis, S., and Schatzmann, M.: Study of line source characteristics for 2-D physical modelling of pollutant dispersion in street canyons, Journal of Wind Engineering and Industrial Aerodynamics, 62, 37–56, 1996.

Molemaker, M. J. and Vilà-Guerau de Arellano, J.: Control of chemical reactions by convective turbulence in the boundary layer, Journal of the atmospheric sciences, 55, 568–579, 1998.

Park, S.-B., Baik, J.-J., Raasch, S., and Letzel, M. O.: A large-eddy simulation study of thermal effects on turbulent flow and dispersion in and above a street canyon, Journal of Applied Meteorology and Climatology, 51, 829–841, 2012.

Park, S.-J., Kim, J.-J., Kim, M. J., Park, R. J., and Cheong, H.-B.: Characteristics of flow and reactive pollutant dispersion in urban street canyons, Atmospheric Environment, 108, 20–31, 2015.

Parra, M., Santiago, J., Martín, F., Martilli, A., and Santamaría, J.: A methodology to urban air quality assessment during large time periods of winter using computational fluid dynamic models, Atmospheric Environment, 44, 2089–2097, 2010.

Santiago, J. and Martilli, A.: A dynamic urban canopy parameterization for mesoscale models based on computational fluid dynamics Reynolds-averaged Navier–Stokes microscale simulations, Boundary-layer meteorology, 137, 417–439, 2010.

Santiago, J. and Martín, F.: SLP-2D: A new Lagrangian particle model to simulate pollutant dispersion in street canyons, Atmospheric Environment, 42, 3927–3936, 2008.

Santiago, J., Krayenhoff, E., and Martilli, A.: Flow simulations for simplified urban configurations with microscale distributions of surface thermal forcing, Urban Climate, 9, 115–133, 2014.

Seinfeld, J. H. and Pandis, S. N.: Atmospheric chemistry and physics: from air pollution to climate change, John Wiley & Sons, 1998.

Stockwell, W. R., Kirchner, F., Kuhn, M., and Seefeld, S.: A new mechanism for regional atmospheric chemistry modeling, Journal of geophysical research: Atmospheres, 102, 25 847–25 879, 1997.

Tominaga, Y. and Stathopoulos, T.: Numerical simulation of dispersion around an isolated cubic building: model evaluation of RANS and LES, Building and Environment, 45, 2231–2239, 2010.

Vardoulakis, S., Fisher, B. E., Pericleous, K., and Gonzalez-Flesca, N.: Modelling air quality in street canyons: a review, Atmospheric environment, 37, 155–182, 2003.

Table 1. The complex chemical mechanism (CCM-CFD): The units of the rate constants of first order reactions are s^{-1}, of second order reactions cm^3s^{-1}. The rate constants for the reactions called "thermal" can be calculated by $k = A * exp[(-E/R)/T]$, of reactions called "Troe" by $k = \{k_0(T)[M])/(1 + (k_0(T)[M]/k_\infty(T))\}0.6^{\{1+[\log_{10}(k_0(T)[M]/k_\infty(T))]^2\}^{-1}}$, and reactions called "Troe-equilibrium" by $k = Aexp(-B/T) \times \{k_0(T)[M]/(1 + (k_0(T)[M]/k_\infty(T)))\}\ 0.6^{\{1+\log_{10}[k_0(T)[M]/k\infty(T)]^2\}^{-1}}$, where $k_0(T) = {k_0}^{300}(T/300)^{-n}$ and $k_\infty(T) = {k_\infty}^{300}(T/300)^{-m}$.

NO_2	NO + O_3	photodissociation
O_3	O^1D	photodissociation
HCHO	CO	photodissociation
HCHO	CO + 2 HO_2	photodissociation
ALD	CO + HO_2 + MO_2	photodissociation
O^1D + N_2	O_3	thermal(A=1.80E-11, E/R=-110.0)
O^1D + O_2	O_3	thermal(A=3.20E-11, E/R=-70.0)
O^1D + H_2O	2 HO	thermal(A=2.20E-10, E/R=0.0)
HO + NO_2	HNO_3	troe(${k_0}^{300}$=2.60E-30, n=3.2,${k_\infty}^{300}$=2.40E-11, m=1.3)
HO_2 + NO	NO_2 + HO	thermal(A=3.70E-12, E/R=-250.0)
O_3 + NO	NO_2	thermal(A=2.00E-12, E/R=1400.0)
HO + SO_2	HO_2	troe(${k_0}^{300}$=3E-31, n=3.3, ${k_\infty}^{300}$=1.50E-12, m=0.0)
CO + HO	HO_2	K = 1.5d-13*(1.+2.439e-20*airc)
ALK + HO	0.931 XO2 + 0.842 HO_2 + 0.011 CO + 0.011 HO + 0.019 HCHO + 0.051 MO2 + 0.378 ALD + 0.096 XO2N	thermal(A=8.05E-12, E/R=237.0)
OLE + HO	1.001 XO2 + 0.998 HO_2 + 1.011 HCHO + 0.002 ACO3 + 0.747 ALD	thermal(A=5.69E-12, E/R=-474.5)
ARO + HO	0.950 XO2 + 0.950 HO_2 + 1.860 ALD + 0.050 XO2N	thermal(A=5.35E-12, E/R=-355.0)
ALD + HO	ACO3	thermal(A=5.55E-12, E/R=-331.0)
HCHO + HO	HO_2 + CO	thermal(A=1.00E-11, E/R=0.0)
OLE + O_3	0.344 HO_2 + 0.383 CO + 0.303 HO + 0.135 XO2 + 0.682 HCHO + 0.092 MO2 + 0.007 ACO3 + 0.630 ALD	thermal(A=1.28E-15, E/R=907.1)
NO_2 + ACO3	PAN	troe(${k_0}^{300}$=9.70E-29, n=5.6,${k_\infty}^{300}$=9.30E-12, m=1.5)
PAN	NO_2 + ACO3	troe-equil (${k_0}^{300}$=9.70E-29, n=5.6, ${k_\infty}^{300}$=9.30E-12, m=1.5, A=1.16E28, B=13954.)
XO2 + NO	NO_2	thermal(A=4.00E-12, E/R=0.0)
MO2 + NO	NO_2 + HO_2 + HCHO	thermal(A=4.20E-12, E/R=-180.0)
ACO3 + NO	NO_2 + 0.046 HO_2 + 0.046 CO + 0.954 MO2	thermal(A=2.00E-11, E/R=0.0)
XO2N + NO	0.939 ONIT	thermal(A=4.45E-12, E/R=-39.9)

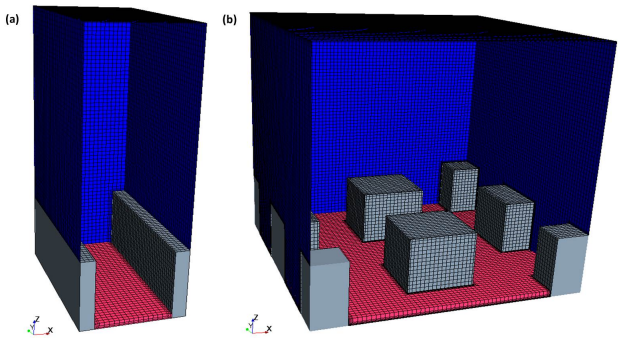

Figure 1. Illustration of the computational domains: (a) a single street canyon with H=16 m and W=16 m (2D-geometry), and (b) staggered array of cubes with H, W and L equal to 16 m (3D-geometry).

Table 2. Summary of all cases simulated in the 2D and 3D geometries. The four chemical scenarios are simulated in each atmospheric condition.

Chemical Scenarios		
Non-reactive		
Photostationary Steady State		
CCM-CFD with VOC/NO_x=1/5 (CCM1/5)		
CCM-CFD with VOC/NO_x=1/2 (CCM1/2)		
Atmospheric Conditions		
	Background $[O_3]$	Reference velocity
Case 1	$[O_3]$=39.8 ppb	u_τ=0.45 m s^{-1}
Case 2	$[O_3]$=39.8 ppb	u_τ=0.23 m s^{-1}
Case 3	$[O_3]$=10.6 ppb	u_τ=0.45 m s^{-1}
Case 4	$[O_3]$=10.6 ppb	u_τ=0.23 m s^{-1}

Table 3. Statistic metrics obtained for the validation of CFD results with experimental data (Meroney et al., 1996) and the acceptance criteria proposed by (Chang and Hanna, 2005) for urban configuration.

	Acceptance Criteria	Statics Values
NMSE	< 1.5	0.03
FB	(-0.3,0.3)	0.068
R	$>$0.8	0.92

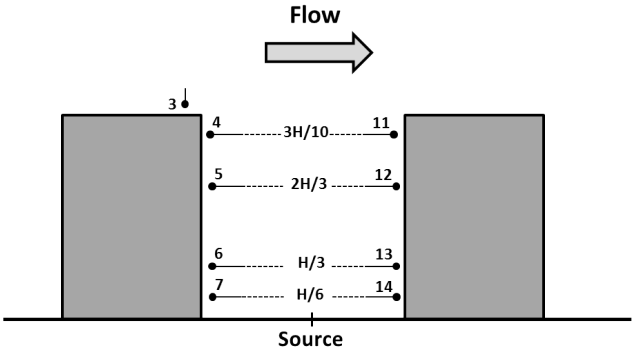

Figure 2. Location of the comparison points with experimental measurements of Meroney et al. (1996)

Table 4. Quadratic relative differences of concentration different time step (%).

	$\mathrm{QD}(\mathrm{t_s} = 0.1\mathrm{s})$	$\mathrm{QD}(\mathrm{t_s} = 2\mathrm{s})$
NO	0.0061	0.023
NO_2	0.0062	0.022
O_3	0.0014	0.0055

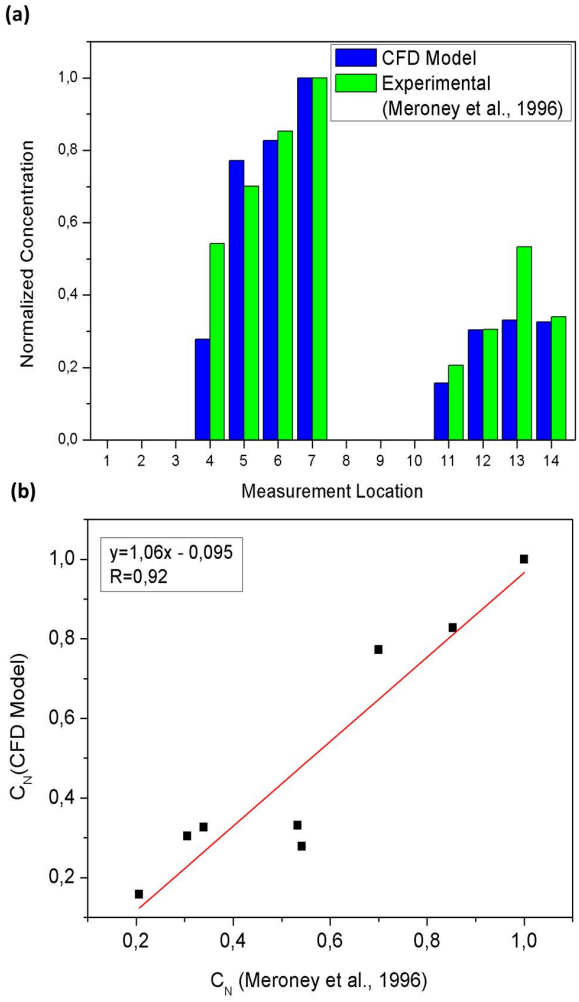

Figure 3. Comparison between simulation results and experimental data (Meroney et al., 1996). (a) Comparison between modeled concentration and experimental measurements at each location. (b) Linear fit between experimental measurements and modeled concentrations.

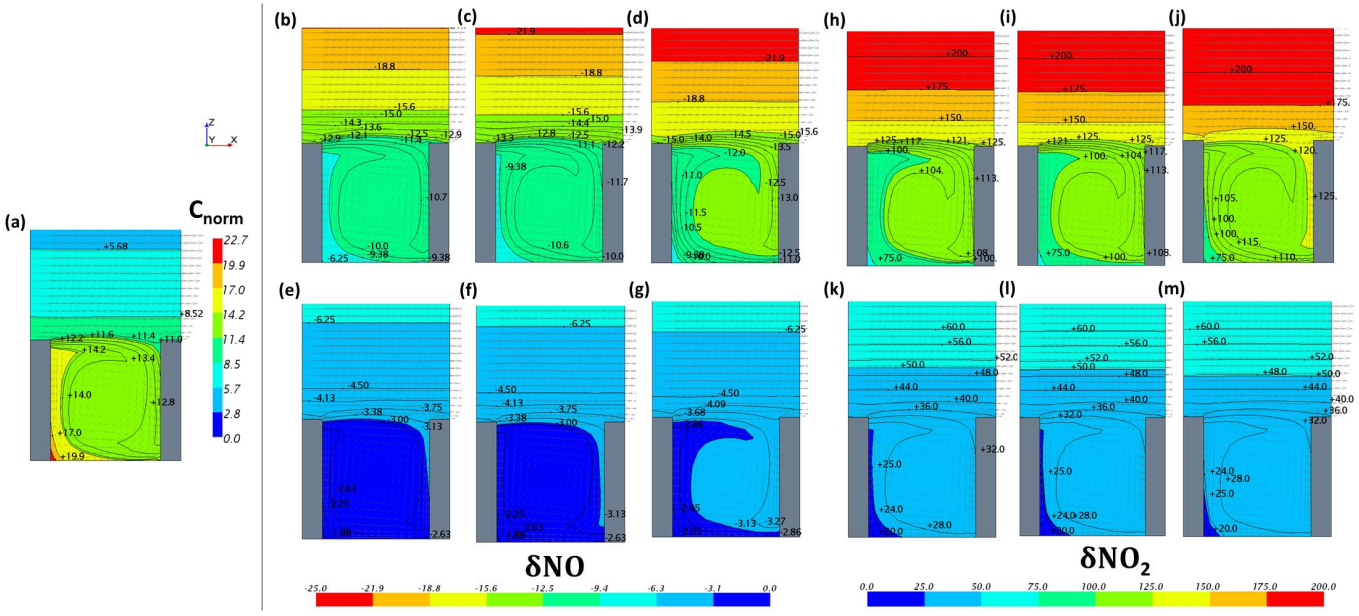

Figure 4. In the 2D-geometry: (a) Distribution of the normalized concentration of tracer and (b-m) the δNO (δNO_2) for PSS, CCM1/5 and CCM1/2 are respectively depicted in b-d (h-j) for the Case 2 and in e-g (k-m) for the Case 4.

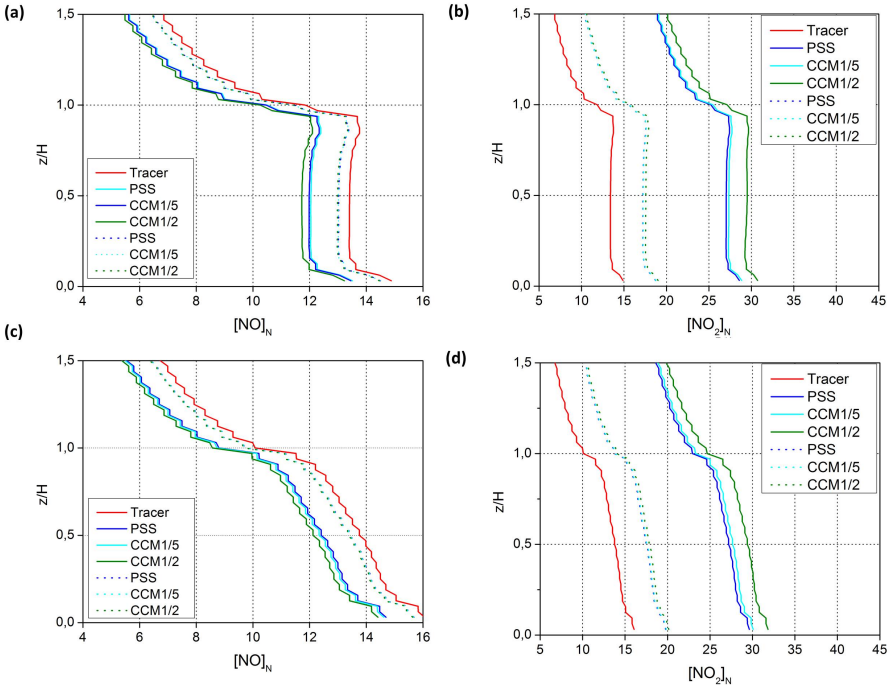

Figure 5. Vertical profiles of horizontal spatial average of $[\mathrm{NO}]_\mathrm{N}$ and $[\mathrm{NO_2}]_\mathrm{N}$ for all chemical scenarios in Case 2 (solid line) and Case 4 (dotted line) in both geometries: 2D (a,b) and 3D (c,d).

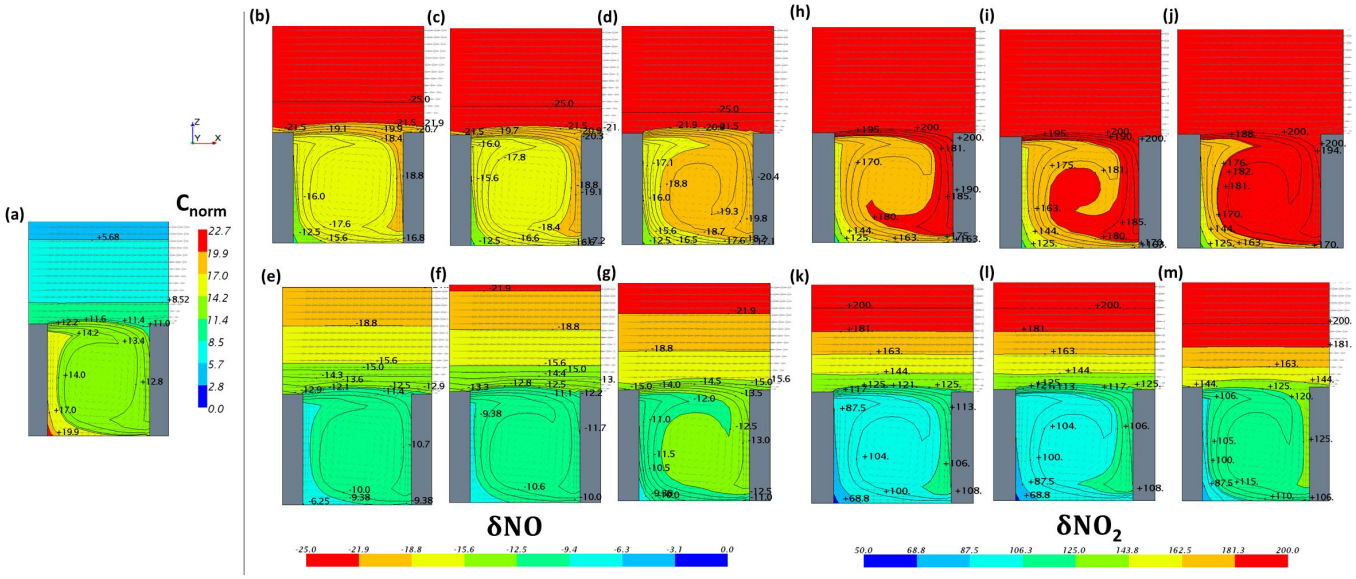

Figure 6. In the 2D-geometry: (a) Distribution of normalized concentration of tracer and (b-m) the $\delta\mathrm{NO}$ ($\delta\mathrm{NO_2}$) for the PSS, CCM1/5 and CCM1/2 are respectively depicted in b-d (h-j) for the Case 1 and in e-g (k-m) for the Case 2.

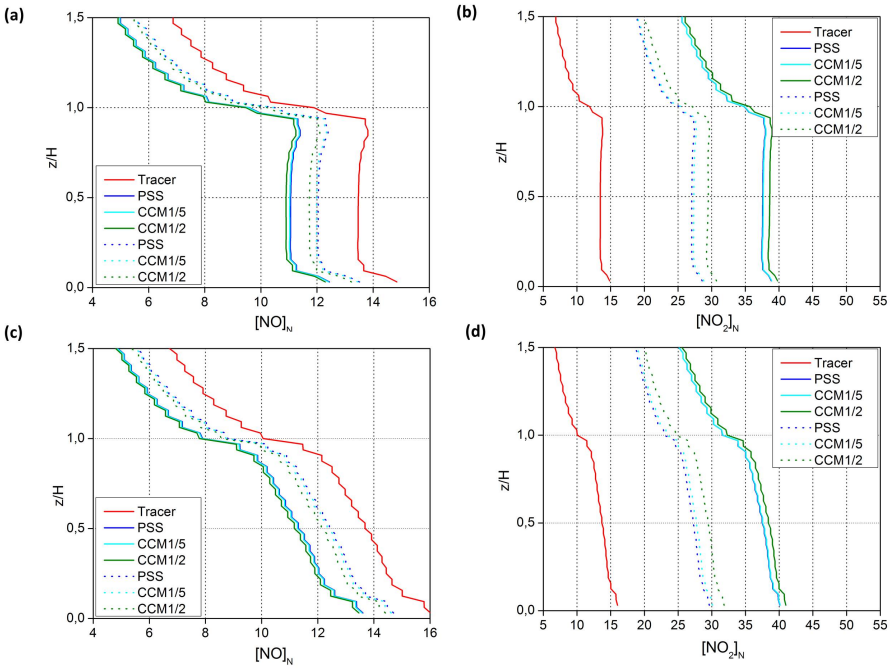

Figure 7. Vertical profiles of horizontal spatial average of $[\mathrm{NO}]_\mathrm{N}$ and $[\mathrm{NO_2}]_\mathrm{N}$ for all chemical scenarios in Case 1 (solid line) and Case 2 (dotted line) in both geometries: 2D (a,b) and 3D (c,d).

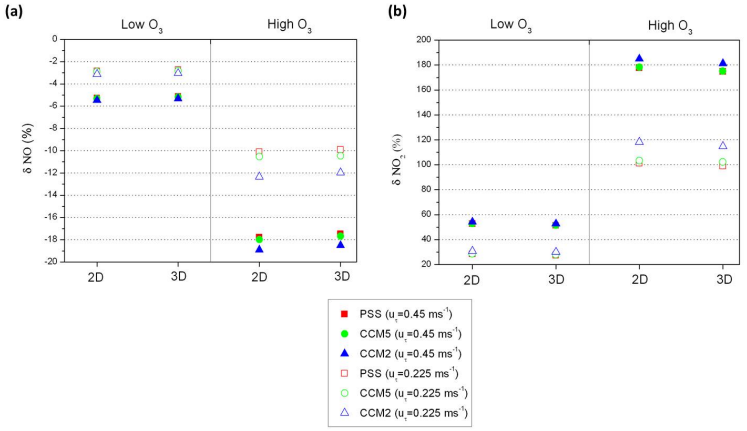

Figure 8. Deviation $[\mathrm{NO}]_\mathrm{N}$ and $[\mathrm{NO_2}]_\mathrm{N}$ in average below the canopy top with respect to its corresponding normalized concentration averaged of the tracer in 2D and 3D geometry.

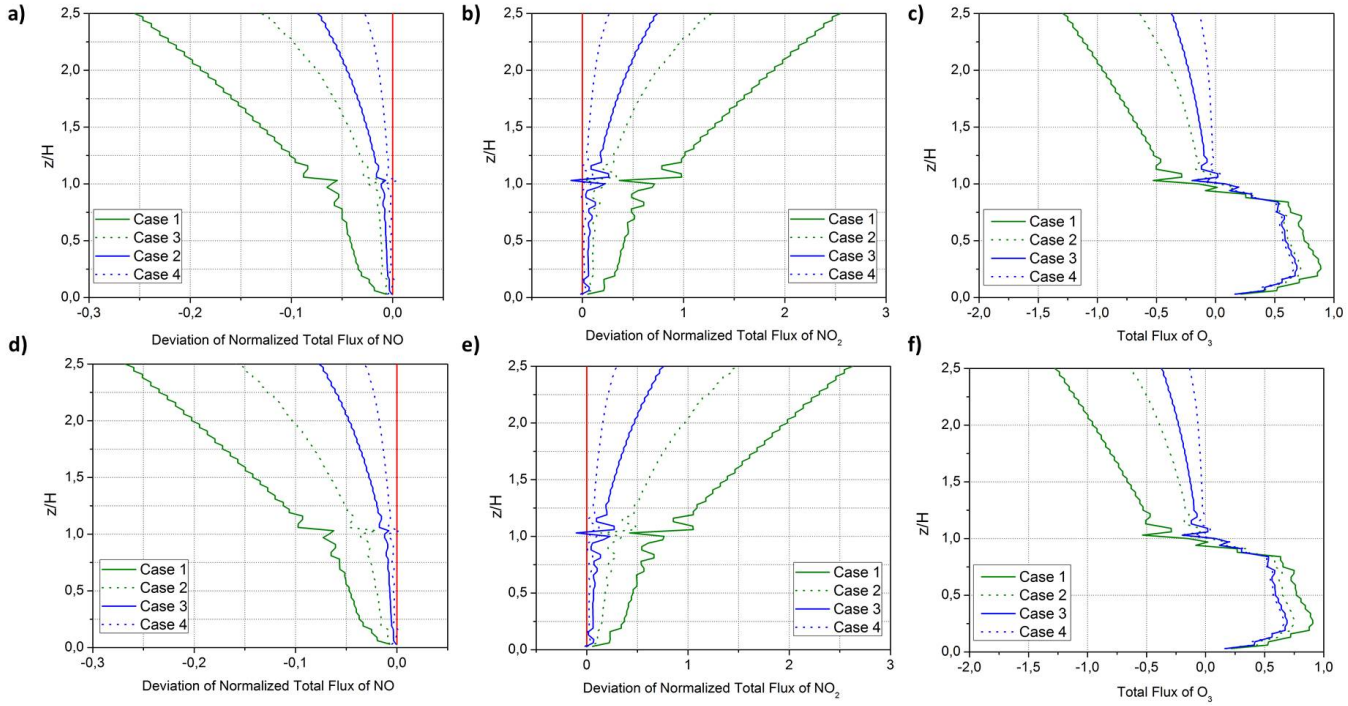

Figure 9. Vertical profiles of the the deviation of $< \overline{w\,\mathrm{NO}} >_\mathrm{N}$ and $< \overline{w\,\mathrm{NO_2}} >_\mathrm{N}$ from the normalized total flux of tracer and the $< \overline{w\,\mathrm{O_3}} >_\mathrm{N}$ for the (a-c) PSS and (d-f) CCM1/2 in the 3D geometry for all study cases. The red line is the normalized total flux of the tracer.

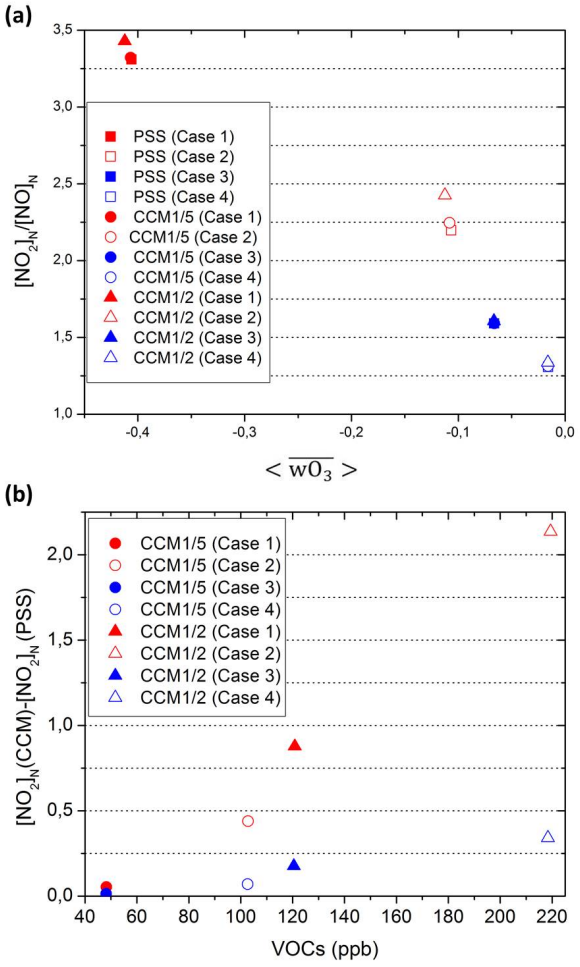

Figure 10. (a) The average concentration within the canopy of $[NO_2]_N/[NO]_N$ against the total flux of O_3 at roof level and (b) the variation of the average concentration within the canopy of $[NO_2]_N$ with CCM1/5 and CCM1/2 from that the PSS over the average concentration of VOC.